Available online at www.sciencedirect.com
SCIENCE DIRECT
Chemical Engineering and Processing 45 (2006) 874–885
Chemical Engineering and Processing
www.elsevier.com/locate/cep

# Control of batch crystallization—A system inversion approach

Ulrich Vollmer [a], Jörg Raisch [a,b,*]

[a] *Systems and Control Theory Group, Max-Planck-Institut für Dynamik komplexer technischer Systeme, Sandtorstr. 1, D-39106 Magdeburg, Germany*
[b] *Fachgebiet Regelungssysteme, Institut für Energie- und Automatisierungstechnik, Fakultät IV, Technische Universität Berlin, Einsteinufer 17, D-10587 Berlin, Germany*

Received 20 September 2005; received in revised form 31 January 2006; accepted 31 January 2006
Available online 6 March 2006

**Abstract**

In this article, a new approach to the control of batch cooling crystallizers is presented. In batch cooling crystallization, the crucial control problem is to design a temperature trajectory which produces a desired crystal size distribution at the end of the batch. Traditionally, this problem is addressed in an optimization framework. Here, a completely different solution is presented. It is shown that the standard population balance model can be inverted analytically. System inversion is performed making use of a state-dependent time scaling of the population balance model. Consequently, for any achievable crystal size distribution at the end of the batch, the corresponding temperature trajectory can be determined in a straightforward way as a feedforward control signal. Furthermore, exploiting the properties of the corresponding time-scaled moment model, a nonlinear feedback controller is designed for the batch crystallizer to ensure tracking of the previously generated feedforward trajectories in the presence of uncertainty.


*Keywords:* Batch crystallization; Population balance model; Process control; Orbital flatness

## 1. Introduction

Crystallization is an important step in many complex production processes in the chemical industries. In batch mode, it is mostly used for the production of small amounts of high-value-added fine chemicals and pharmaceuticals. Batch operation provides a high degree of flexibility and allows for rapidly changing product specifications and quality requirements. The operation of a single plant in several different ways to meet changing product specifications requires the ability to quickly determine appropriate control strategies which achieve prespecified product requirements.

Product specifications for crystalline substances include the desired crystal size distribution (CSD), which may be specified in several different ways. It may either be entirely determined as a function of crystal size, or it may only be required to have certain properties (e.g. a certain mean crystal size). A third way to describe a desired product CSD is to define an objective function which is to be optimized (e.g. maximizing mean crystal size). In this contribution, the first two possibilities are treated. In all three cases, the control problem is to determine how to operate the crystallizer during a batch run such that a desired CSD is obtained at the end of the batch. This is, first of all, a problem of trajectory planning and feedforward control. In a second step, it is desirable to incorporate feedback to be able to react to disturbances during the operation and to eliminate the effects of model uncertainties.

In this article, more specifically, batch *cooling* crystallization is considered. Cooling crystallization exploits the fact that solubility depends on temperature. The initially undersaturated hot solution is cooled during batch operation. Since solubility decreases with temperature the solution becomes supersaturated. Supersaturation is the driving force for nucleation and crystal growth, the main mechanisms involved in crystallization. As the rates of nucleation and crystal growth depend on the degree of supersaturation, and supersaturation, in turn, is a function of temperature, the final product CSD can be influenced by the temperature–time-profile during the batch. Consequently, crystallizer temperature, or, if its dynamics cannot be neglected, the temperature of the cooling jacket, serves as the manipulated

* Corresponding author.
*E-mail address:* raisch@mpi-magdeburg.mpg.de (J. Raisch).

0255-2701/$ – see front matter © 2006 Elsevier B.V. All rights reserved.
doi:10.1016/j.cep.2006.01.012

variable for batch cooling crystallizers. The first part of the overall control problem is then to determine a feedforward control scheme, i.e. a temperature signal which produces a desired CSD at the end of the batch. The second part, as indicated above, is the synthesis of an adequate feedback controller.

Crystallization processes can be adequately described by *population balance models* [1,2]. These are distributed parameter systems typically consisting of a partial differential equation (PDE) describing the evolution of the CSD, which is a function of time and crystal size, coupled with one or more ordinary differential equations (ODE) for concentration and temperature of the liquid phase. The population balance model considered in this article is of a standard type frequently found in the crystallization literature, see e.g. Randolph and Larson [1]; Rawlings et al. [3]. The formulation used here is taken from Miller and Rawlings [4] and is presented in Section 2. Its specific form implies that a finite-dimensional moment model can be derived that exactly describes the dynamics of a number of leading moments of the CSD.

Based on a population balance model, it is of course possible to determine the final product CSD for a given temperature profile by simulation. The inverse problem, i.e. the computation of a feedforward control signal producing a desired CSD, is of course much harder. See Fig. 1 for an illustration of the inverse problem. In the literature, the problem of batch crystallizer control has been addressed mainly from an optimization point of view. A number of authors, such as Ajinkya and Ray [5]; Jones [6]; Ulrich [7]; Mayrhofer and Nyvlt [8]; Miller and Rawlings [4]; Lang et al. [9], have considered the problem of finding a temperature trajectory which maximizes or minimizes a characteristic of the final CSD. These studies differ with respect to model assumptions, optimization methods, objective functions and the question whether or not constraints can be handled. The methods applied vary from Pontryagin's maximum principle to nonlinear dynamic optimization. Concerning the underlying process models, in actual case studies, moment models (or even simpler equations) have been used, although the more recent approaches could certainly also handle population balance models. Since an optimal temperature signal represents an open loop control law, the positive effects may be lost due to plant-model mismatch or because of imperfect tracking of the desired optimal temperature trajectory. This issue is treated by Ma and Braatz [10]. Attempts to incorporate feedback in the optimal control of batch cooling crystallizers can be found in Chang and Epstein [11]; Motz et al. [12]; Zhang and Rohani [13]. The influence of the distribution of seed crystals and its use as a further degree of freedom for optimization is studied by Chung et al. [14]. Optimization of a CSD over more than one characteristic crystal length has recently been considered by Ma and Braatz [15].

If the objective is to obtain large crystals, it is beneficial to suppress nucleation as far as possible such that seed crystals grow to larger sizes. Therefore, Mullin and Nývlt [16] derived a temperature trajectory to maintain nucleation at a constant low level. Because of the nonlinear dependence of nucleation and growth rates on supersaturation it is also possible to favour growth over nucleation by keeping supersaturation at a constant low value. This is another popular approach, which has been pursued, e.g., by Jones and Mullin [17] in an open loop setting. Xie et al. [18] designed a nonlinear feedback controller for the same purpose. The usage of fines dissolution as an additional manipulated variable for batch crystallizer control has been examined by Jones and Chianese [19]; Rohani et al. [20].

In Section 3 of this article, a different approach is presented. It is neither based on optimisation, nor does it just keep one process variable constant. The approach presented there uses methods from nonlinear control theory to analytically determine the feedforward control signal that steers the system into a desired final CSD. More specifically, based on a state-dependent time scaling, a procedure is developed which allows inversion of the system model and hence can be used to check whether a desired final CSD is physically possible and, if so, to compute the corresponding temperature signal. A control theoretic interpretation of these results has been previously given by the authors of this article [21]. In Section 4, the properties of the time-scaled system model are further exploited to design trajectories that achieve certain CSD properties (expressed in terms of moments of the CSD) at the end of the batch. Finally, a feedback control scheme to track such a trajectory in the presence of uncertainty is presented in Section 5.

## 2. Population Balance Model for the batch crystallizer

A batch cooling crystallizer is depicted in Fig. 2. It is operated as follows. Initially the vessel is filled with hot undersaturated solution. Then, the crystallizer is cooled such that the liquid becomes supersaturated. At this point, small seed crystals may be added. Due to supersaturation, new crystals are formed and existing crystals grow. Nucleation and growth consume solute

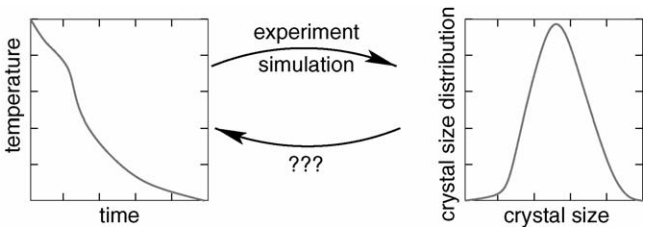


Fig. 1. Illustration of inverse problem.

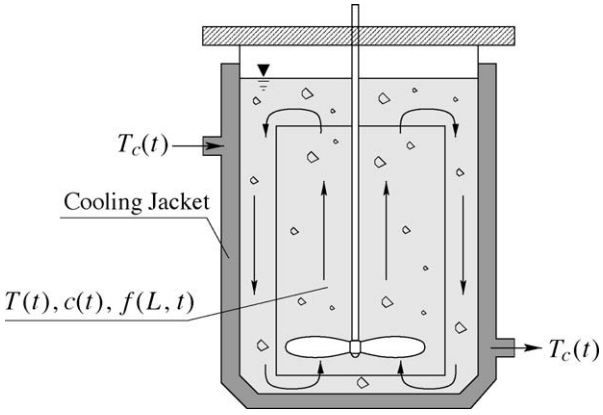


Fig. 2. Sketch of a batch cooling crystallizer.

from the solution such that the concentration decreases. Hence, further cooling is necessary to keep the liquid supersaturated. To prevent settling of crystals, the slurry is mixed by an impeller. At the end of the batch, the vessel is discharged and the crystalline product undergoes further processing steps such as filtering and drying. The quality of the product as well as the efficiency of downstream processing is heavily influenced by the CSD.

For process modelling, the size of crystals is defined by a characteristic length $L$. The CSD is described by the number density function $f(L,t)$, which represents the number of crystals per crystal length $L$ and volume of slurry $V$. In the following, a batch crystallizer model is presented which is standard in the crystallization literature. The specific formulation used here is taken from Miller and Rawlings [4]. The underlying assumptions are that all crystals grow at the same rate, i.e. the growth rate $G$ is independent of crystal size, and that nuclei are formed at negligible size. Furthermore, attrition, breakage and agglomeration of crystals is neglected. Balancing the number of crystals in an infinitesimal interval of crystal length, a PDE is obtained which, together with appropriate initial and boundary conditions, describes the temporal evolution of the CSD:

$$\frac{\partial f(L,t)}{\partial t} = -\frac{\partial (G(t) f(L,t)}{\partial L} \tag{1a}$$

$$f(0,t) = \frac{B(t)}{G(t)} \tag{1b}$$

$$f(L,0) = f_{\text{seed}}(L). \tag{1c}$$

The rate of nucleation is denoted by $B(t)$ and $f_{\text{seed}}(L)$ is the CSD of seed crystals added at the beginning of the batch. Eq. (1a) is called the *population balance*. For details of crystallizer modelling see Randolph and Larson [1]. A mole balance for the liquid phase yields an ordinary differential equation for the solute concentration $c(t)$,

$$\frac{\mathrm{d}c(t)}{\mathrm{d}t} = -3\rho_{\text{c}} k_v h \int_0^\infty L^2 G(t) f(L,t) \mathrm{d}L, \tag{2}$$

with $c(0) = c_0$, where $\rho_{\text{c}}$ is the density of crystals, $h$ a conversion factor equal to the volume of slurry per mass of solvent, and $k_v$ a volume shape factor defined such that the volume of a crystal with length $L$ is $V_{\text{crystal}}(L) = k_v L^3$. Furthermore, an ODE for the temperature $T(t)$ is obtained from an energy balance of the crystallizer:

$$\rho V c_{\text{p}}(t) \frac{\mathrm{d}T(t)}{\mathrm{d}t} = -3\Delta H_{\text{c}}(t) \rho_{\text{c}} k_v V \int_0^\infty L^2 G(t) f(L,t) \mathrm{d}L - UA_{\text{c}}(T(t) - T_{\text{c}}(t)) \tag{3}$$

with $T(0) = T_0$. $T_{\text{c}}(t)$ is the temperature of the cooling jacket, $UA_{\text{c}}$ represents the product of heat-transfer coefficient and heat-transfer area, and $\rho$ the density of the slurry. The heat of crystallization, $\Delta H_{\text{c}}$, depends on solution concentration $c(t)$. This dependence can be adequately represented by a quadratic term,

$$\Delta H_{\text{c}}(t) = B_0 + B_1 c(t) + B_2 c(t)^2, \tag{4}$$

where the coefficents $B_i$, $i = 0, \ldots, 2$, are fitted to empirical data. Similarly, the heat capacity of the solution as a function of solution concentration can be expressed as:

$$c_{\text{p}}(t) = C_0 + C_1 \left( \frac{c(t)}{1 + c(t)} \right) + C_2 \left( \frac{c(t)}{1 + c(t)} \right)^2. \tag{5}$$

The dependence of nucleation and growth rates on supersaturation $S(t)$ and CSD $f(L,t)$ is modelled by:

$$G(t) = k_g S(t)^g, \tag{6}$$

$$B(t) = k_b S(t)^b k_v \int_0^\infty L^3 f(L,t) \mathrm{d}L, \tag{7}$$

where supersaturation $S(t)$ is defined as:

$$S(t) = \frac{c(t) - c_{\text{sat}}(t)}{c_{\text{sat}}(t)}. \tag{8}$$

The dependence of saturation concentration $c_{\text{sat}}$ on temperature $T$ is represented approximately by a second-order expression of the form:

$$c_{\text{sat}}(t) = A_0 + A_1 T(t) + A_2 T(t)^2. \tag{9}$$

The growth and nucleation laws (6), (7) are empirical relations *not* derived directly from first principles. Values for the parameters $k_g$, $k_b$, $g$ and $b$ have to be identified from measurements from the specific plant to be modelled. The parameters depend on the material to be crystallized, the crystallizer geometry and operating conditions, whereas $A_0$, $A_1$ and $A_2$ are solely determined by the combination of solute and solvent substances.

Eqs. (1a)–(9) constitute an infinite-dimensional model for the batch crystallizer. The model basically consists of the first-order PDE (1a) with boundary condition (1b) and initial condition (1c), coupled with two ODEs (2) and (3). The CSD is characterized by its moments:

$$\mu_i(t) = \int_0^\infty L^i f(L,t) \mathrm{d}L, \qquad i = 0, 1, 2, \ldots \tag{10}$$

Some of the moments have a clear physical interpretation. For example, the zeroth moment $\mu_0(t)$ gives the overall number of crystals, the second moment $\mu_2(t)$ is proportional to the overall crystal surface, and the third moment $\mu_3(t)$ is proportional to the volume of the crystalline material in the crystallizer. As the duration of the batch is finite and the growth rate $G(t)$ is bounded, $f(L,t)$ is zero for large enough $L$. Hence, by integration in parts, it follows from (1a), (1b) that:

$$\frac{\mathrm{d}\mu_0(t)}{\mathrm{d}t} = B(t)$$

$$\frac{\mathrm{d}\mu_i(t)}{\mathrm{d}t} = iG(t)\mu_{i-1}(t), \qquad i = 1, 2, \ldots \tag{11}$$

Since the overall mass of solute in the crystallizer, dissolved plus crystalline, is constant, there is an additional algebraic relation between the third moment $\mu_3(t)$ and the solute concentration $c(t)$

$$c(t) = c_0 + \rho_{\text{c}} k_v h (\mu_{3,\text{seed}} - \mu_3(t)) \tag{12}$$

where $\mu_{3,\text{seed}} = \int_0^\infty L^3 f_{\text{seed}}(L)\mathrm{d}L$ is the third moment of the seed CSD. Furthermore, note that the integral expression in the nucleation law (7) is the third moment, i.e.

$$B(t) = k_b k_v S(t)^b \mu_3(t). \tag{13}$$

Because of (8), (6), (9) and (12), $B(t)$ and $G(t)$ are entirely determined by $\mu_3(t)$ and $T(t)$. Hence, the differential equations for the first four moments and the crystallizer temperature can be written as:

$$\frac{\mathrm{d}\mu_0(t)}{\mathrm{d}t} = B(\mu_3(t), T(t)) \tag{14a}$$

$$\frac{\mathrm{d}\mu_1(t)}{\mathrm{d}t} = G(\mu_3(t), T(t))\mu_0(t) \tag{14b}$$

$$\frac{\mathrm{d}\mu_2(t)}{\mathrm{d}t} = 2G(\mu_3(t), T(t))\mu_1(t) \tag{14c}$$

$$\frac{\mathrm{d}\mu_3(t)}{\mathrm{d}t} = 3G(\mu_3(t), T(t))\mu_2(t) \tag{14d}$$

$$\frac{\mathrm{d}T(t)}{\mathrm{d}t} = -\frac{3\rho_c k_v}{\rho}\frac{\Delta H_c(\mu_3(t))G(\mu_3(t), T(t))\mu_2(t)}{c_p(\mu_3(t))} - \frac{UA_c}{\rho V}\frac{(T(t) - T_c(t))}{c_p(\mu_3(t))} \tag{14e}$$

with initial conditions

$$\mu_i(0) = \mu_{i,\text{seed}} = \int_0^\infty L^i f_{\text{seed}}(L)\mathrm{d}L,$$
$$i = 0, \ldots, 3, \quad T(0) = T_0.$$

This constitutes a simplified model for the batch crystallizer. It is clearly nonlinear, but finite-dimensional. The moments $\mu_0(t) \ldots \mu_3(t)$ and temperature $T(t)$ are the states of the simplified model, and cooling jacket temperature $T_c(t)$ is its control input. This model exactly describes the dynamics of the first four moments of the CSD but it does of course not describe the evolution of the entire CSD. However, as will be seen in the following section, both model formulations – infinite-dimensional population balance model and finite-dimensional moment model – play their specific role in the feedforward control design.

## 3. Feedforward control by system inversion

In this section, the crystallizer temperature $T$ is considered to be the control input, as the temperature dynamics is usually fast and can therefore be often neglected in batch crystallization processes. Hence, the problem is to determine which temporal evolution of $T$ will achieve a desired CSD at the end of the batch. As a first step towards the solution of this system inversion problem, consider the characteristic lines of the PDE (1a). By definition, $f(L,t)$ is constant on these lines, i.e.

$$\frac{\mathrm{d}f(L,t)}{\mathrm{d}t} = \frac{\partial f(L,t)}{\partial L}\frac{\mathrm{d}L}{\mathrm{d}t} + \frac{\partial f(L,t)}{\partial t} = 0. \tag{15}$$

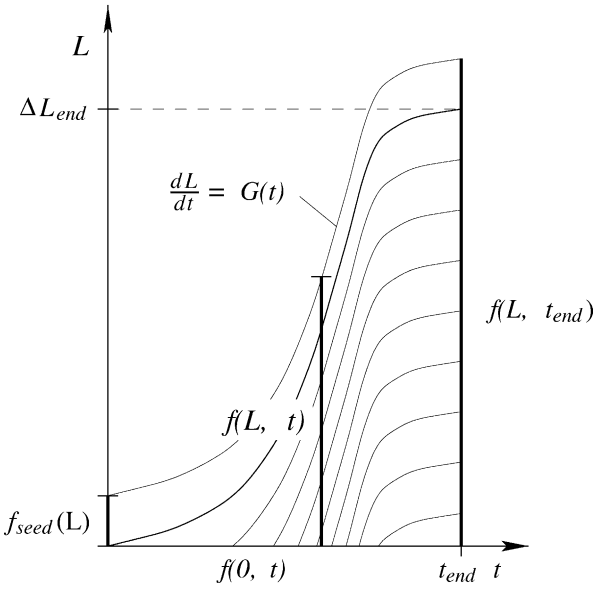


Fig. 3. Characteristic lines of PDE model (1a).

Using (1a), this results in the following expression for the characteristic lines:

$$\frac{\mathrm{d}L}{\mathrm{d}t} = G(t). \tag{16}$$

An illustration is given in Fig. 3, where the CSD can be visualized as a surface over the $(L,t)$ plane, with the contour lines given by the characteristic lines. It is obvious from Fig. 3 that the characteristic lines relate the CSD at the end of the batch, $f(L,t_{\text{end}})$, to $f(0,t)$, i.e. the number of nuclei during the batch. Hence, in principle, it should be possible to translate the final CSD (which is a function of crystal size $L$) to $f(0,t)$, a function of time. However, at this point, it is not yet clear how to formulate this relation mathematically. To do this, a time scaling is introduced by defining a new 'time'-variable $\tau$:

$$[\,t_0 \quad t_{\text{end}}\,] \mapsto [\,\tau_0 \quad \tau_{\text{end}}\,]$$
$$\mathrm{d}\tau = G\,(\mu_3(t), T(t))\,\mathrm{d}t, \quad \tau(t_0) = \tau_0. \tag{17}$$

Since the growth rate satisfies

$$0 < G(\mu_3(t), T(t)) < \infty, \quad \forall t \tag{18}$$

the mapping from $t$ to $\tau$ is bijective. Hence, the time transformation is invertible, and a control law designed in new time $\tau$ can be transformed back and applied in real time $t$. Because of (18), $\tau$ is a monotonically increasing function in $t$ and goes to infinity if and only if $t$ goes to infinity—properties that are intuitively expected in the concept of 'new time'.

In new time $\tau$, the population balance (1a) becomes a simple transport type equation,

$$\frac{\partial f(L,\tau)}{\partial \tau} = -\frac{\partial f(L,\tau)}{\partial L}. \tag{19}$$

This implies that $f(L,\tau)$ is constant on straight lines in the $(L,\tau)$-domain with $\mathrm{d}L/\mathrm{d}\tau = 1$, see Fig. 4. Now, it is a simple exercise to mathematically formulate the relation between the final CSD

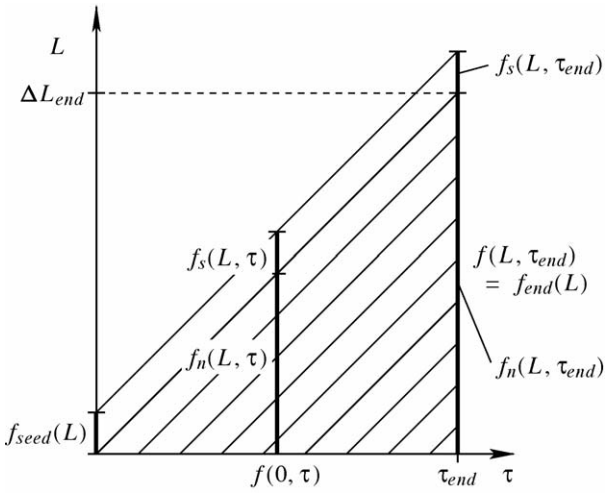


Fig. 4. Characteristic lines of PDE model (19).

and the time profile of the boundary value of the CSD, $f(0,\tau)$. From Fig. 4 it is obvious that:

$$f(0, \tau) = f_{\text{end}}(\tau_{\text{end}} - \tau), \quad 0 < t \leq \tau_{\text{end}}. \tag{20}$$

Using the boundary condition (1b) it follows that:

$$\frac{B(\tau)}{G(\tau)} = f_{\text{end}}(\tau_{\text{end}} - \tau). \tag{21}$$

Hence, it is now easily possible to translate a desired final CSD $f_{\text{end},d}(L)$ into the corresponding time profile $(B(\tau)/G(\tau))_d$. This concludes the first step of the system inversion.

In a second step, we need to determine the temperature signal $T(\tau)$ corresponding to the desired quotient $B(\tau)/G(\tau)$. To this end, we apply the time scaling (17) to the moment model (14a)–(14e) and get:

$$\frac{\mathrm{d}\mu_0(\tau)}{\mathrm{d}\tau} = \frac{B(\mu_3(\tau), T(\tau))}{G(\mu_3(\tau), T(\tau))} \tag{22a}$$

$$\frac{\mathrm{d}\mu_1(\tau)}{\mathrm{d}\tau} = \mu_0(\tau) \tag{22b}$$

$$\frac{\mathrm{d}\mu_2(\tau)}{\mathrm{d}\tau} = 2\mu_1(\tau) \tag{22c}$$

$$\frac{\mathrm{d}\mu_3(\tau)}{\mathrm{d}\tau} = 3\mu_2(\tau) \tag{22d}$$

$$\frac{\mathrm{d}T(\tau)}{\mathrm{d}\tau} = -\frac{3\rho_c k_v}{\rho}\frac{\Delta H_c(\mu_3)\mu_2}{c_p(\mu_3)} - \frac{UA_c}{\rho V}\frac{T - T_c}{G(\mu_3, T)c_p(\mu_3)} \tag{22e}$$

If the desired evolution $(B(\tau)/G(\tau))_d$ of the quotient $(B(\tau)/G(\tau))$ is known (as a result of the first step), it is obvious that this function has to be integrated four times with respect to time $\tau$ to obtain the desired evolution of the third moment, $\mu_{3,d}(\tau)$. Taking into account initial conditions, we get

$$\mu_{3,d}(\tau) = 6\int\int_0^\tau\int\int f_{\text{end},d}(\tau_{\text{end}} - \theta)\mathrm{d}\theta^4 + \mu_{3,\text{seed}} + 3\mu_{2,\text{seed}}\tau + 3\mu_{1,\text{seed}}\tau^2 + \mu_{0,\text{seed}}\tau^3. \tag{23}$$

Inserting this result and the definitions of growth and nucleation rates into Eq. (21) yields:

$$\left(\frac{B(\mu_{3,d}(\tau), T_d(\tau))}{G(\mu_{3,d}(\tau), T_d(\tau))}\right)_d = f_{\text{end},d}(\tau_{\text{end}} - \tau), \tag{24}$$

in which temperature $T_d(\tau)$ is the only unknown. This is a quadratic equation in $T_d$, given the quadratic dependence of saturation concentration $c_{\text{sat}}$ on temperature in Eq. (9). Eq. (24) has two solutions:

$$T_d(\tau) = \frac{-A1 \pm \sqrt{A_1^2 - 2A_0A_2 + 4A_2c_d(\tau)(1 + (k_g f_{\text{end},d}(\tau_{\text{end}} - \tau)/(hk_bk_v\mu_{3,d}(\tau)))^{1/(b-g)})^{-1}}}{2A_2} \tag{25}$$

of which only the positive one is physically meaningful.

This concludes the second step of system inversion. It provides the temperature evolution corresponding to a desired product CSD $f_{\text{end},d}(L)$. However, this evolution is a function of new time $\tau$. Hence, the time transformation (17) has to be inverted to obtain the desired temperature evolution, $T_d$, in original time. This requires the evaluation of the integral:

$$t = \int_0^\tau \frac{1}{G(\mu_{3,d}(\theta), T_d(\theta))}\mathrm{d}\theta \tag{26}$$

and the solution of the resulting equation for $\tau$. Depending on the kinetic relations used for the growth and nucleation rate and the function chosen for the desired CSD $f_{\text{end},d}(L)$, these computations may be done analytically or numerically. If inversion of the time transformation can be done analytically, an explicit functional dependence of temperature $T_d$ on time $t$ is obtained. Otherwise, $T_d(t)$ can only be determined at a number of time instances. However, this is not a severe restriction for practical implementation.

The system inversion procedure discussed in this section involves three main steps. The first step uses the fact that the time-scaled population balance model exhibits straight-line characteristics. The second step exploits an invertibility property of the time scaled moment model. In the control theory literature, this property is referred to as *differential flatness*. It was introduced by Fliess et al. [22,23] and applied to problems from chemical engineering, e.g. by Rothfuß et al. [24]. The moment model (14a)–(14d) is called *orbitally flat* since the time-scaled model is differentially flat. For more details on orbital flatness, see Fliess et al. [25]; Respondek [26]; Guay [27]. The third and last step is the inversion of the time scaling. The three steps are illustrated in Fig. 5.

**Example.** For illustration, the procedure is applied to a specific example. The batch crystallizer is supposed to be started with a

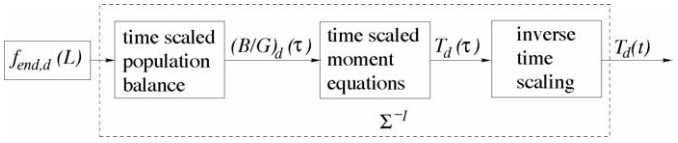


Fig. 5. Steps involved in the system inversion.

solution of concentration:

$$c_0 = 0.493 \frac{g_{KNO_3}}{g_{H_2O}} \tag{27}$$

which corresponds to a saturation temperature of 32 °C. A small amount ($m_{seed} = 0.05$ g) of seed crystals of size $L_{seed} = 196$ μm is added, i.e. the initial number density function is:

$$f_{seed}(L) = \frac{N_{seed}}{V} \delta(L - L_{seed}), \tag{28}$$

where $\delta(\cdot)$ is the Dirac impulse and the number of seed crystals is:

$$N_{seed} = \frac{m_{seed}}{\rho_c k_v L_{seed}^3}. \tag{29}$$

For a complete list of model parameter values and operating conditions see Miller and Rawlings [4].

From Fig. 3, it is obvious that it is only possible to shape $f(L,t_{end})$ by an appropriate cooling policy if $L < \Delta L_{end}$. For $L \geq \Delta L_{end}$, one simply obtains the crystals from the seed CSD uniformly grown in size by $\Delta L_{end}$. As an example, suppose the desired final distribution is $Ae^{-BL}$ for $L < \Delta L_{end}$, i.e.

$$f_{end,d}(L) = \begin{cases} Ae^{-BL} & \text{for } L < \Delta L_{end} \\ \dfrac{N_{seed}}{V} \delta(L - (L_{seed} + \Delta L_{end})) & \text{for } L \geq \Delta L_{end} \end{cases} \tag{30}$$

with $A$ and $B$ two positive real parameters.

From the desired final CSD $f_{end,d}(L)$ and Eq. (20), the corresponding temporal evolution $f_d(L=0,\tau)$ is obtained as:

$$\left(\frac{B(\tau)}{G(\tau)}\right)_d = f_d(0,\tau) = f_{end,d}(\tau_{end} - \tau) = Ae^{-B(\tau_{end}-\tau)},$$
$$0 < \tau \leq \tau_{end}. \tag{31}$$

According to Eq. (23), the desired evolution of the third moment is:

$$\mu_{3,d}(\tau) = \frac{Ae^{-B\tau_{end}}(6e^{B\tau} - B^3\tau^3 - 3B^2\tau^2 - 6B\tau - 6)}{B^4} + \frac{N_{seed}(L_{seed} + \tau)^3}{V}. \tag{32}$$

The desired temperature signal is determined by inserting (30) and (32) into Eq. (25). For the sake of brevity, the resulting expression is not given explicitly here. Finally, the time transformation has to be inverted according to Eq. (26)

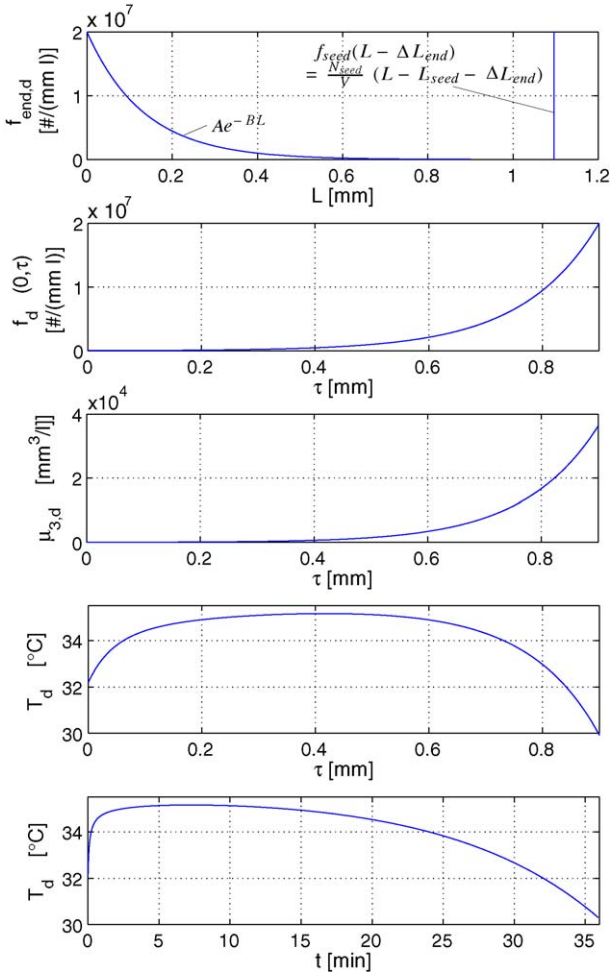


Fig. 6. Desired final CSD and corresponding temporal evolution of boundary condition, third moment and temperature.

This integral has to be evaluated and the resulting equation has to be solved for $\tau$. Inserting the function $\tau(t)$ in Eq. (25) yields the desired temperature signal $T$ in original time. However, the integral in (33) cannot be evaluated analytically. Hence, temperature $T$ cannot be obtained as an explicit function of time $t$, but values at an arbitrary number of time instants can be determined by numerical evaluation of (33). Results are illustrated in Fig. 6 for the following set of parameter values: $A = 2 \times 10^7$ (mm l)$^{-1}$, $B = 7.5$ mm$^{-1}$, $\Delta L_{end} = 0.9$ mm. The figure shows the evolution of $f_d(0,\tau)$, of the third moment $\mu_{3,d}(\tau)$ and of temperature $T_d(\tau)$, all in new time $\tau$. It also shows the desired temperature signal $T_d$ in original time.

## 4. Feedforward control for desired csd properties

In the previous section, it was shown how to determine an appropriate feedforward control signal, i.e. a suitable tem-

$$t = \int_0^\tau \frac{1}{G(\mu_{3,d}(\theta), T_d(\theta))} d\theta = \int_0^\tau \left[ \frac{\left( \frac{AB^4 e^{B\theta} k_g V}{h k_b k_v} (B^4 e^{BL_{end}} N_{seed}(L_{seed} + \theta)^3 - AV(6(1 - e^{B\theta}) + 6B\theta + 3B^2\theta^2 + B^3\theta^3)) \right)^{-1} }{k_g} \right]^{-g/(b-g)} d\theta \tag{33}$$

poral evolution of the crystallizer temperature, if the desired CSD is completely specified as a function of crystal size. In this case, where the entire shape of the CSD $f_{\mathrm{end},d}(L)$ is fixed, there is only one solution to the feedforward control problem, i.e. there is exactly one temperature signal generating the desired CSD.

In this section, we investigate the case where the function $f_{\mathrm{end},d}(L)$ is not completely fixed, but only certain properties, formulated in terms of the moments of the CSD, are specified at the end of the batch. In this case, there is also a certain degree of freedom when determining an appropriate feedforward control signal.

As only moments of the CSD are within the scope of this section, it is sufficient to work with the moment model (14a)–(14e). Again, as in the previous section, invertibility of the time-scaled moment model (22a)–(22e), i.e. its differential flatness, is exploited. A flat system possesses a so-called *flat output*, which completely characterizes the dynamic behaviour of the system. More specifically, the temporal evolution of all system states and the system input(s) can be computed from the flat output signal and a finite number of its time derivatives without solving differential equations. Clearly, this is a very convenient property for trajectory planning and control design. The flat output signal can be smoothly parameterized, e.g. by a polynomial, in new time $\tau$. The coefficients can then be determined such that the signal is compatible with given initial conditions and with the desired properties of the final CSD. Due to the property of the flat output, it is then straightforward to compute the corresponding evolution of all system states and the control input.

As an example, consider the problem of steering the system from an initial condition characterized by (27), (28) to a CSD where the weight mean size

$$L_{wm} = \frac{\mu_4}{\mu_3}, \tag{34}$$

the overall crystal mass, $m_{\mathrm{end}} = k_v \rho_c V \mu_3$, and the maximum length of nucleated crystals, $\Delta L_{\mathrm{end}}$, are prescribed. Since the definition of the weight mean size $L_{wm}$ involves the fourth moment $\mu_4$, the equation:

$$\frac{\mathrm{d}\mu_4(t)}{\mathrm{d}t} = 4G(\mu_3(t), T(t))\mu_3(t) \tag{35}$$

has to be added to the model (14a)–(14e). Similarly, the time-scaled model (22a)–(22e) is augmented by the equation:

$$\frac{\mathrm{d}\mu_4(\tau)}{\mathrm{d}\tau} = 4\mu_3(\tau). \tag{36}$$

The resulting sixth-order model is flat with the highest, i.e. the fourth moment serving as a flat output

$$y(\tau) = \mu_4(\tau). \tag{37}$$

In a first step, it is now shown how to invert this system model, i.e. how to determine the system input from the flat output and its time derivatives. Afterwards, in a second step, it is shown how to determine an appropriate flat output for the given specifications.

Differentiating the flat output $y$ six times with respect to new time $\tau$ yields:

$$\frac{\mathrm{d}y(\tau)}{\mathrm{d}\tau} = 4\mu_3(\tau) \tag{38a}$$

$$\frac{\mathrm{d}^2y(\tau)}{\mathrm{d}\tau^2} + 12\mu_2(\tau) \tag{38b}$$

$$\frac{\mathrm{d}^3y(\tau)}{\mathrm{d}\tau^3} = 24\mu_1(\tau) \tag{38c}$$

$$\frac{\mathrm{d}^4y(\tau)}{\mathrm{d}\tau^4} = 24\mu_0(\tau) \tag{38d}$$

$$\frac{\mathrm{d}^5y(\tau)}{\mathrm{d}\tau^5} = 24\frac{B(\mu_3(\tau), T(\tau))}{G(\mu_3(\tau), T(\tau))} \tag{38e}$$

$$\frac{\mathrm{d}^6y(\tau)}{\mathrm{d}\tau^6} = 4\phi(\mu_3(\tau), \mu_2(\tau), T(\tau), T_c(\tau)) \tag{38f}$$

where

$$\phi(\mu_3, \mu_2, T, T_c) = 6\frac{G(\mu_3, T)((\partial B/\partial T)(\partial T/\partial\tau) + (\partial B/\partial\mu_3)(\mathrm{d}\mu_3/\mathrm{d}\tau)) - B(\mu_3, T)((\partial G/\partial T)(\mathrm{d}T/\mathrm{d}\tau) + (\partial G/\partial\mu_3)(\mathrm{d}\mu_3/\mathrm{d}\tau))}{G(\mu_3, T)^3}. \tag{39}$$

with the expressions for $\mathrm{d}\mu_3/\mathrm{d}\tau$ and $\mathrm{d}T/\mathrm{d}\tau$ according to (22d) and (22e), respectively. Note that $\phi(\mu_3, \mu_2, T, T_c)$ is affine with respect to the system input $T_c$, i.e. it is of the form:

$$\phi(\mu_3, \mu_2, T, T_c) = \alpha(\mu_3, \mu_2, T) + \beta(\mu_3, T)T_c. \tag{40}$$

From (37), (38a)–(38d) it is immediately clear that the states $\mu_4(\tau) \ldots \mu_0(\tau)$ can be computed from $y(\tau)$ and its first four derivatives. The state $T(\tau)$ can be determined from (38e) by additionally using the fifth derivative. Finally, the computation of the input $T_c(\tau)$ from Eq. (38f) also involves the sixth derivative of the flat output. If temperature $T$ is used as the control input, which is common practice in batch crystallizer control, the sixth derivative (38f) is not needed for system inversion. In this case, Eq. (38e) is solved for the input $T$, using (38a) to replace $\mu_3$. This is done in the following way. Using the expressions for growth and nucleation rates given in Eqs. (6) and (7), Eq. (38e) is solved for supersaturation:

$$S(\tau) = \left(\frac{k_g y^{(5)}(\tau)}{6hk_bk_v y'(\tau)}\right)^{\frac{1}{b-g}}. \tag{41}$$

Then, the definition of supersaturation (8) together with the expression for the saturation concentration (9) is solved for temperature $T$. Due to the quadratic dependence in (9) this, as in (25), yields two solutions for $T$ of which only the positive one

is physically meaningful

$$T(\tau) = -\frac{A_1}{2A_2} + \frac{\sqrt{A_1^2(1+S(\tau)) - 4A_2(A_0 - c(\tau) + A_0 S(\tau))}}{2A_2\sqrt{1+S(\tau)}}. \tag{42}$$

In this solution, $S(\tau)$ can be replaced by a function of the flat output $y(\tau)$ and its derivatives using (41) and $c(\tau)$ is replaced using (12) and (38a). Hence, this constitutes the desired system inversion. For any desired evolution $y_d(\tau)$ of the flat output $y(\tau)$, the corresponding input trajectory $T_d(\tau)$ can be calculated. If this feedforward control signal is to be applied in "real" time $t$, the time scaling has to be inverted by (numerically) integrating (26) and solving for $\tau$.

In a second step, the problem of trajectory planning is treated. We determine a flat output signal such that the system evolves from the initial state to a final state satisfying the specifications. For this purpose, the desired flat output signal $y_d(\tau)$ is parameterized by an eighth-order polynomial in new time $\tau$

$$y_d(\tau) = \sum_{i=0}^{8} a_i \tau^i. \tag{43}$$

The six leading coefficients $a_0 \ldots a_5$ are determined such that $y_d(\tau)$ is consistent with the initial values for the moments $\mu_0 \ldots \mu_4$ and the initial value of supersaturation $S$, which is determined by the initial values for solute concentration $c_0$ and temperature $T_0$:

$$y_d(0) = a_0 = \mu_4(0) \tag{44a}$$

$$y_d'(0) = a_1 = 4\mu_3(0) \tag{44b}$$

$$y_d''(0) = 2a_2 = 12\mu_2(0) \tag{44c}$$

$$y_d'''(0) = 6a_3 = 24\mu_1(0) \tag{44d}$$

$$y_d^{(4)}(0) = 24a_4 = 24\mu_0(0) \tag{44e}$$

$$y_d^{(5)}(0) = 120a_5 = \frac{24B(\tau=0)}{G(\tau=0)}. \tag{44f}$$

The prime in $y_d'$ denotes differentiation with respect to $\tau$. Furthermore, the following final time conditions are to be met:

$$L_{wm}(\tau_{\text{end}}) = \frac{\mu_4(\tau_{\text{end}})}{\mu_3(\tau_{\text{end}})} = \frac{4y_d(\tau_{\text{end}})}{y_d'(\tau_{\text{end}})} = 500\,\mu\text{m}, \tag{45a}$$

$$m(\tau_{\text{end}}) = k_v\rho_c V\mu_3(\tau_{\text{end}}) = \frac{k_v\rho_c V}{4} y_d'(\tau_{\text{end}}) = 50\,\text{g} \tag{45b}$$

$$\Delta L_{\text{end}} = \tau_{\text{end}} = 800\,\mu\text{m}. \tag{45c}$$

This, overall, constitutes a system of nine equations for 10 unknown parameters (nine coefficients $a_0, \ldots, a_8$ and final time $\tau_{\text{end}}$). Hence, a family of solutions is obtained, one of which can be chosen, e.g., such that supersaturation, crystallizer temperature or batch time remain within certain bounds. In Fig. 7, trajectories resulting from different choices of the free coefficient $a_8$ are shown. From the requirements (45a) and (45b) it follows that all trajectories reach the same value of weight mean size $L_{\text{wm}}$ and fourth moment $\mu_4$ (i.e. flat output $y$) at final time $t_{\text{end}}$. The final values of temperature $T$ and supersaturation $S$ may differ. As can be seen from the figure, batch time $t_{\text{end}}$ decreases

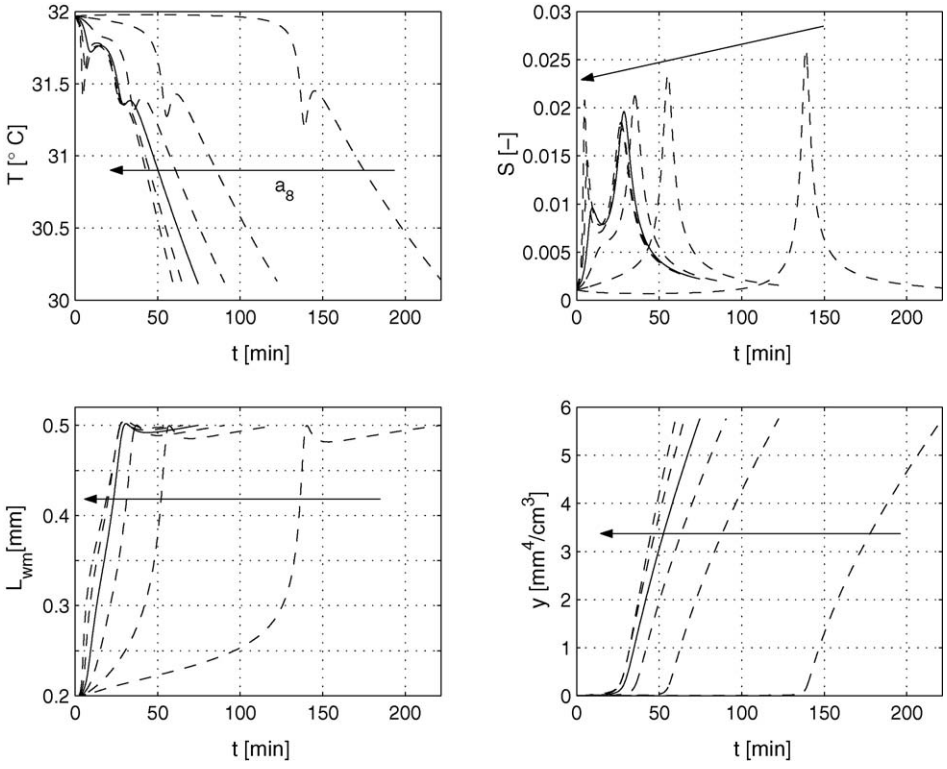


Fig. 7. Desired evolution of temperature $T$, supersaturation $S$, weight mean size $L_{wm}$ and flat output $y = \mu_4$ (top left—bottom right) for different values of coefficient $a_8$.

with $a_8$. Also, the maximum temperature gradient observed during the batch changes depends on $a_8$. For very small and very large values of $a_8$ the maximum temperature gradient is unrealistically high. Hence, these trajectories have to be ruled out. A good choice for the free parameter is, e.g., $a_8 = 30\,\mathrm{mm}^{-4}\,\mathrm{cm}^{-3}$, corresponding to the solid curves in Fig. 7. For this choice all variables remain in a reasonable range. In the following section, a feedback tracking controller is designed to stabilize the system around the desired trajectory resulting from this choice.

## 5. Nonlinear feedback tracking control

Beside their invertibility property, which can be exploited for trajectory planning and design of feedforward control, flat systems possess a further advantage. They are linearizable by feedback. Based on this property it is possible to synthesize feedback controllers for the stabilization of batch crystallization processes around desired trajectories resulting, for example, from the feedforward control design procedures in Sections 3 and 4.

In the following, as an example, a tracking controller is designed to stabilize the crystallizer around the reference trajectory determined in Section 4. Recall that this trajectory takes the system from a given initial condition to a final CSD where weight mean size $L_{wm}(t_{\mathrm{end}})$, crystal mass $m_{\mathrm{end}}$ and final size of seed crystals $\Delta L_{\mathrm{end}}$ are specified. Since the definition of weight mean size $L_{\mathrm{wm}}$ involves the fourth moment $\mu_4$, the crystallizer model (14a)–(14e) is augmented by Eq. (36). As pointed out in Section 4, $y = \mu_4$ is a flat output of the augmented model.

As the function $\phi$ defined in (39) is affine in $T_{\mathrm{c}}$, the feedback law:

$$T_{\mathrm{c}} = \frac{0.25v - \alpha(\mu_3, \mu_2, T)}{\beta(\mu_3, T)} \tag{46}$$

with $\alpha$ and $\beta$ according to (39), (40), exactly linearizes the nonlinear batch crystallizer model. Inserting (46) into (38f), the feedback linearized system is obtained as:

$$\frac{\mathrm{d}^6 y}{\mathrm{d}\tau^6} = v, \tag{47}$$

with $v$ a fictitious input and $y$ the flat output. Asymptotic tracking of the desired output signal $y_d(\tau)$ is accomplished by a simple linear control law for the input $v$

$$v = y_d^{(6)} - \sum_{i=0}^{5} (q_i (y^{(i)} - y_d^{(i)})) \tag{48}$$

where the coefficients $q_i$ are chosen such that the tracking error dynamics are stable. Eqs. (46) and (48) form a nonlinear tracking controller for the batch crystallizer. The flat output and its derivatives occurring in the control law (48) can be replaced by system states of the original crystallizer model using (38a)–(38f). Thus, (46), (48) form a nonlinear static state feedback controller. The complete system state needs to be measured (or estimated by an observer).

Note that the rate of convergence of the tracking error defined by the coefficients $q_i$ in (48) is with respect to new time $\tau$. Since

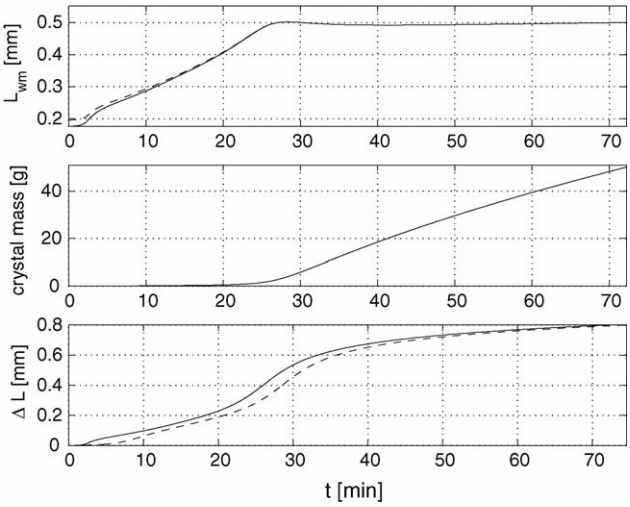


Fig. 8. Weight mean size $L_{\mathrm{wm}}(t)$, crystal mass $m(t)$, and size increase of crystals $\Delta L(t)$, actual (solid line) and desired (dashed line) trajectory.

$\tau$ is associated with crystal size $L$, in real time $t$ the tracking error decays fast when growth rate $G$ is large, the decay is slow when $G$ is low.

For a simulation study, a controller as defined in (46), (48) is implemented with the coefficients $q_i$ chosen such that all six poles of the tracking error dynamics in new time are at $\lambda_k = 20\,\mathrm{mm}^{-1}$, $k = 1, \ldots, 6$. In a first simulation run, an offset at time $t = 0$ is considered. The desired trajectory starts from the initial condition (27), (28) with the exception that the actual initial value of the fourth moment $\mu_4$ is decreased by 10%. Fig. 8 shows the temporal evolution of weight mean size $L_{\mathrm{wm}}(t)$, crystal mass $m(t)$, and size increase of crystals $\Delta L(t)$. These are the quantities involved in the final time requirements for the desired trajectory (45a)–(45c). Fig. 9 presents the corresponding evolution of supersaturation $S(t)$, crystallizer temperature $T(t)$ and temperature of cooling jacket $T_{\mathrm{c}}(t)$. In Fig. 10, the tracking error is plotted versus original time $t$ and new time $\tau$. It can be seen that in new time $\tau$ the error dynamics exhibits the expected sixth-

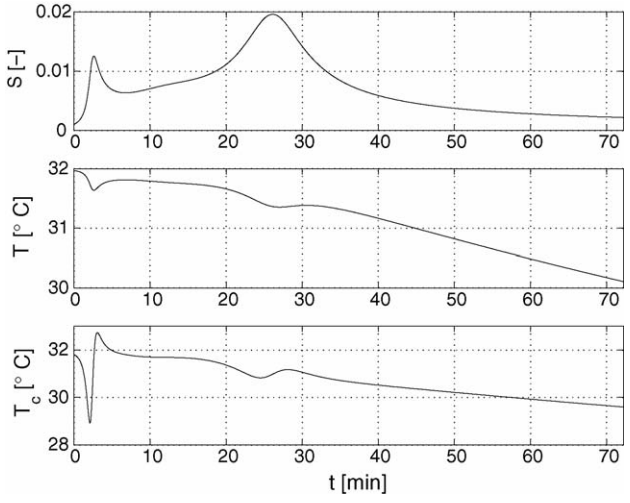


Fig. 9. Supersaturation $S(t)$, crystallizer temperature $T(t)$ and cooling jacket temperature $T_{\mathrm{c}}(t)$.

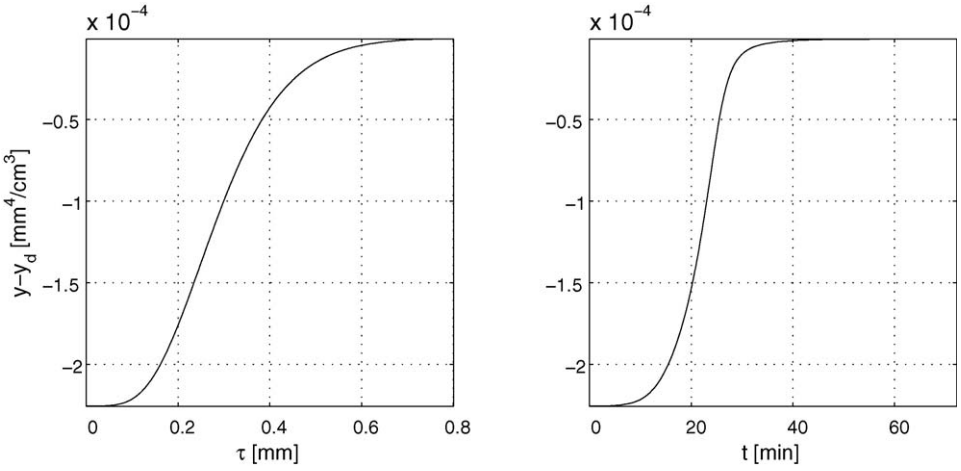


Fig. 10. Tracking error $y - y_d$ vs. new time $\tau$ and vs. original time $t$.

order linear decay behaviour, whereas in original time $t$ the error decays quickly during the time span $20\,\text{min} < t < 30\,\text{min}$, i.e. when supersaturation (and therefore growth rate) is large.

In a second simulation run, in addition to the initial offset a model error is taken into account. The most uncertain part of the model is the nucleation rate as defined in Eq. (7). Nucleation is hard to capture since several mechanisms contribute to this phenomenon. Furthermore, it is heavily influenced by impurities in the solution. Therefore, to demonstrate the performance of the tracking controller in the presence of model errors, the nucleation rate parameter $k_b$ is increased by 20%. Again, the same plots are presented as for the previous simulation. In Fig. 11, it can be seen that the final time requirements on weight mean size $L_{\text{wm}}(t_{\text{end}})$, crystal mass $m(t_{\text{end}})$ and length increase $\Delta L(t_{\text{end}})$ are met quite precisely. The trajectories of supersaturation $S(t)$, crystallizer temperature $T(t)$ and cooling jacket temperature $T_c(t)$ in Fig. 12 are changed only slightly compared to the case without model error (see Fig. 9). However, there are two main differences.

First, the absolute tracking error $y(t) - y_d(t)$ in Fig. 13 obviously does not converge to 0 any more. It can be shown that instead of the nominal error dynamics resulting from (47) and (48) a modified error equation is obtained with the modified nucleation rate $\bar{B} = k_{\text{err}} B$

$$y^{(6)} = k_{\text{err}} \left( y_d^{(6)} - q_5 \left( \frac{1}{k_{\text{err}}} y^{(5)} - y_d^{(5)} \right) - \sum_{i=0}^{4} q_i (y^{(i)} - y_d^{(i)}) \right) \tag{49}$$

or equivalently

$$\begin{aligned} (k_{\text{err}} - 1)(y_d^{(6)} + y_d^{(5)}) &= (y^{(6)} - y_d^{(6)}) + q_5 (y^{(5)} - y_d^{(5)}) \\ &\quad + k_{\text{err}} \sum_{i=0}^{4} q_i (y^{(i)} - y_d^{(i)}) \\ &= e^{(6)} + q_5 e^{(5)} + k_{\text{err}} \sum_{i=0}^{4} q_i e^{(i)} \end{aligned} \tag{50}$$

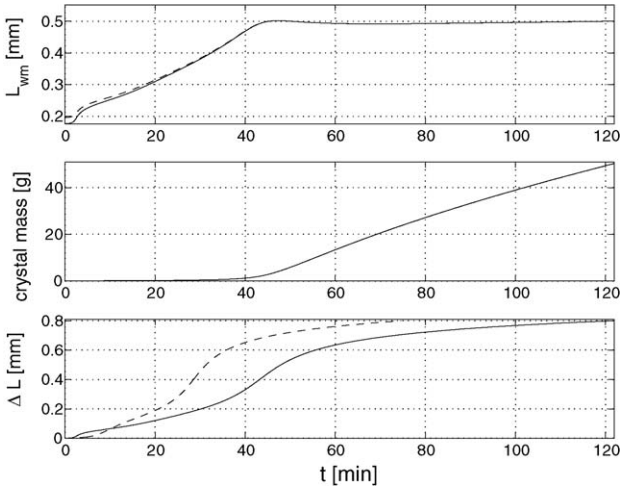


Fig. 11. Weight mean size $L_{\text{wm}}(t)$, crystal mass $m(t)$, and size increase of crystals $\Delta L(t)$, actual (solid line) and desired (dashed line) trajectory, with model error.

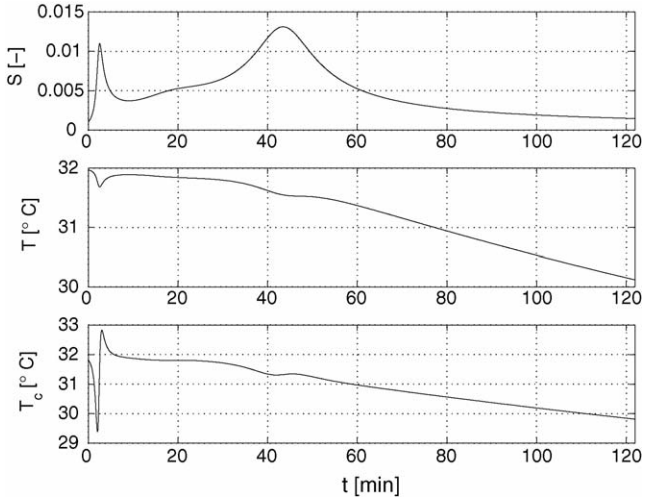


Fig. 12. Supersaturation $S(t)$, crystallizer temperature $T(t)$ and cooling jacket temperature $T_c(t)$, with model error.

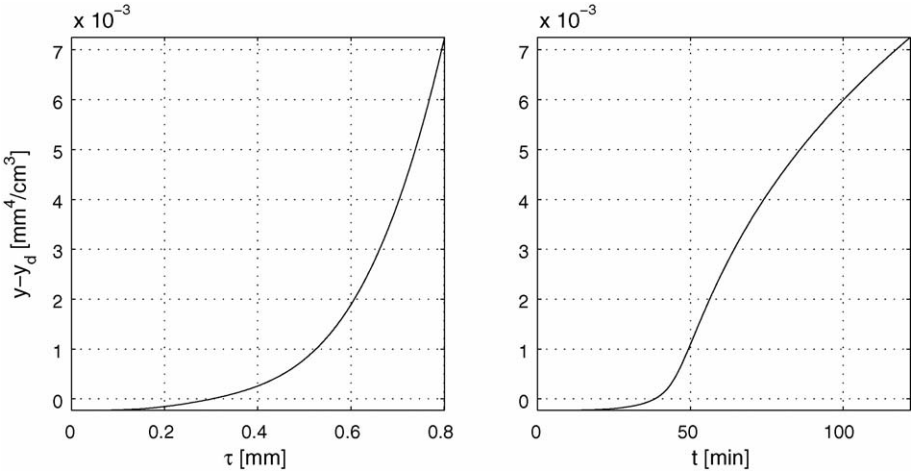


Fig. 13. Tracking error $y - y_d$ vs. new time $\tau$ and vs. original time $t$, with model error.

where $e = y - y_d$. The left hand side of Eq. (50) is a third-order polynomial in $\tau$. If $k_{\mathrm{err}}$ is small enough the error dynamics is still stable and the tracking error $e(t)$ converges to a third-order polynomial. However, as the desired trajectory is an eighth-order polynomial it grows faster than the tracking error, such that the relative tracking error $(y(t)–y_d(t))/y_d(t)$ converges to 0. This also explains the excellent tracking of $L_{\mathrm{wm}}(t)$ and $m(t)$ in Fig. 11.

The second major difference is that the batch time $t_{\mathrm{end}}$ is increased considerably. The desired trajectory in the control law (48) is implemented in new time $\tau$ and it is assumed that $\tau$, which is equivalent to the length increase $\Delta L$, is measurable in the process. Hence, the duration of the batch is not fixed in original time $t$ but in new time $\tau$, i.e. the batch runs until $\tau = \tau_{\mathrm{end}} = \Delta L_{\mathrm{end}}$ is reached. With the model error in the nucleation rate, nucleation is increased. To stay close to the desired trajectory, supersaturation has to be lower than it had to be with the unperturbed model. Hence, the growth rate is lower and, therefore, the duration of the batch has to be longer to achieve the desired length increase $\Delta L_{\mathrm{end}}$.

## 6. Conclusion

In this article, the control of batch crystallization processes was treated in a system inversion framework. It was shown that a state-dependent time scaling can transform a standard batch crystallizer model into a system with very special properties. Namely, the population balance equation of the standard model is transformed to a simple transport type equation with straight-line characteristics, while the corresponding moment model is transformed into a differentially flat system. These properties allow a very elegant design of feedforward and feedback control laws. In Section 3, it was shown that for any achievable final CSD, the corresponding temperature–time profile can be determined by system inversion. In Section 4, differential flatness of the time-scaled moment model was used to plan trajectories and determine a feedforward control signal steering the system from given initial conditions to a product CSD with certain prescribed moment properties. Finally, in Section 5, a nonlinear feedback controller was designed to track desired evolutions of the moments in the presence of model uncertainties. This design procedure exploited the fact that flat systems are exactly linearizable by feedback. The solution to each of these problems was illustrated by a simulation example.

We conclude with a few remarks on the impact of control input constraints, although this topic has not been formally investigated in this article. In the feedback case presented in Section 5, the manipulated variable (coolant temperature $T_{\mathrm{c}}(t)$) exhibits a rather steep peak during the first 5 min of the simulated experiment, see Fig. 9. In fact, its maximum gradient, $\max \mathrm{d}T_{\mathrm{c}}/\mathrm{d}t$, is 7.5 K/min. Of course, the maximum possible temperature gradient is always limited due to physical constraints. Further simulation studies reveal, however, that control is not overly sensitive with regard to rate constraints; for example, control still works properly if the coolant temperature gradient is limited to 3 K/min. The amplitude of the coolant temperature peak becomes larger than in the unconstrained case, but final time constraints are still met perfectly. Of course, if the constraint is tightened even further, the controller will eventually fail to follow the desired trajectory. In this case, the desired trajectory has to be replanned such that at least the open loop control signal meets the constraints. A related topic is how, in the trajectory planning problem in Section 3, constraints on the temperature gradient $\mathrm{d}T/\mathrm{d}t$ affect the achievable shape of the final time CSD, $f_{\mathrm{end}}(L)$. Such constraints limit the maximum slope of $f_{\mathrm{end}}(L)$, but the precise nature of this relation remains to be investigated.

## References

[1] A. Randolph, M. Larson, Theory of Particulate Processes, Academic Press, Inc, 1988.
[2] D. Ramkrishna, Population Balances: Theory and Applications to Particulate Systems in Engineering, Academic Press, 2000.
[3] J. Rawlings, S. Miller, W. Witkowski, Model identification and control of solution crystallization processes: a review, Ind. Eng. Chem. Res. 32 (1993) 1275–1296.
[4] S. Miller, J. Rawlings, Model identification and control strategies for batch cooling crystallizers, AIChE J. 40 (8) (1994) 1312–1327.

[5] M. Ajinkya, W. Ray, On the optimal operation of crystallization processes, Chem. Eng. Comm. 1 (1974) 181–186.
[6] A. Jones, Optimal operation of a batch cooling crystallizer, Chem. Eng. Sci. 29 (1974) 1075–1087.
[7] M. Ulrich, Optimization of batch solution crystallization, Ger. Chem. Eng. 4 (1979) 195–200.
[8] B. Mayrhofer, J. Nyvlt, Programmed cooling of batch crystallizers, Chem. Eng. Process. 24 (1988) 217–220.
[9] Y. Lang, A. Cervantes, L. Biegler, Dynamic optimization of a batch cooling crystallization process, Ind. Eng. Chem. Res. 38 (1999) 1469–1477.
[10] D. Ma, D. Braatz, Worst-case analysis of finite-time control policies, IEEE Trans. Auto. Control 9 (2001) 766–774.
[11] C.-T. Chang, M. Epstein, Simulation studies of a feedback control strategy for batch crystallizers, AIChE Symp. Ser. 83 (1987) 110–119.
[12] S. Motz, J. Eggers, E. Gilles, Model-based operation of batch crystallizers, in: Proceedings of the 15th International Symposium on Ind. Cryst., 3, 2002, pp. 1173–1179.
[13] G. Zhang, S. Rohani, On-line optimal control of a seeded batch crystallizer, Chem. Eng. Sci. 58 (2003) 1887–1896.
[14] S. Chung, D. Ma, R. Braatz, Optimal seeding in batch crystallization, Can. J. Chem. Eng. 77 (1999) 590–596.
[15] D. Ma, D. Braatz, Robust identification and control of batch processes, Comp. Chem. Eng. 27 (2003) 8–9.
[16] J. Mullin, J. Nývlt, Programmed cooling of batch crystallizers, Chem. Eng. Sci. (1971) 26.
[17] A. Jones, J. Mullin, Programmed cooling crystallization of potassium sulphate solutions, Chem. Eng. Sci. 29 (1974) 105–118.
[18] W. Xie, S. Rohani, A. Phoenix, Dynamic modeling and operation of a seeded batch cooling crystallizer, Chem. Eng. Comm. 187 (2001) 229–249.
[19] A. Jones, A. Chianese, Fines destruction during batch crytsallization, Chem. Eng. Comm. 62 (1987) 5–16.
[20] S. Rohani, N. Tavare, J. Garside, Control of crystal size distribution in a batch cooling crystallizer, Can. J. Chem. Eng. 68 (1990) 260–267.
[21] U. Vollmer, J. Raisch, Control of batch cooling crystallisers based on orbital flatness, Int. J. Contr. 76 (16) (2003) 1635–1643.
[22] M. Fliess, J. Levine, P. Martin, P. Rouchon, On Differentially Flat Nonlinear Systems. Nonlinear Control Systems Design, Pergamon Press, 1992, pp. 408–412.
[23] M. Fliess, J. Levine, P. Martin, P. Rouchon, Flatness and defect of nonlinear systems: introductory theory and examples, Int. J. Contr. 61 (1995) 1327–1361.
[24] R. Rothfuß, J. Rudolph, M. Zeitz, Flatness based control of a nonlinear chemical reactor model, Automatica 32 (10) (1996) 1433–1439.
[25] M. Fliess, J. Levine, P. Martin, P. Rouchon, Design of trajectory stabilizing feedback for driftless flat systems, in: Proceedings of the 3rd European Control Conference ECC'95, 3, 1995, pp. 1882–1887.
[26] W. Respondek, Orbital feedback linearization of single-input nonlinear control systems, in: Proceedings of IFAC NOLCOS'98, Enschede, The Netherlands, 1998, pp. 499–504.
[27] M. Guay, An algorithm for orbital feedback linearizaton of single-input control affine systems, Syst. Control Lett. 38 (1999) 271–281.